

Stable particle acceleration in co-axial plasma channels

Alexander Pukhov and John P. Farmer

Institut für Theoretische Physik I, Universität Düsseldorf, 40225 Germany

The attainable transformer ratio in plasma accelerators is limited by instabilities. Using three-dimensional particle-in-cell simulations, we demonstrate that these can be controlled using a hollow plasma channel with a co-axial plasma filament. The driver scatters electrons from the filament, and the slow pinch of the ions leads to a strong chirp of the effective betatron frequency, preventing beam breakup. We demonstrate the monoenergetic acceleration of an electron bunch to 20 GeV over 4.4 m, achieving a transformer ratio of 10, an energy efficiency of 40% and an emittance of $1.8 \mu\text{m}$.

Plasma wakefields [1] offer a potential basis for novel high-energy particle accelerators [2] due to the high field gradients plasma can support. A driver excites a plasma wake, which is in turn used to accelerate a trailing witness bunch. The driver can be either an intense laser pulse [3] or a charged particle bunch [4]. Reaching high energies in both cases is challenging. For a laser driver, the limitation is due to dephasing, as the witness bunch travels faster than the laser driver. This can be overcome by using a staged acceleration [5].

In this work, we focus on the use of a particle driver. One can use short - shorter than the plasma period - drive bunches in quasi-linear [6] or blow-out [7, 8] regimes. Alternatively, one may harness the self-modulation of longer bunches in plasma [9, 10]. For the accelerating medium, one may choose either uniform plasma [4], or a pre-formed plasma channel [11]. Each of these regimes has its own particular advantages and drawbacks.

Perhaps the most promising accelerating scheme is that of the hollow plasma channel [12]. A radially symmetric drive bunch in a cylindrical channel does not generate any focusing or defocusing fields, which would allow the use of a long drive beam, necessary for high transformer ratios, and guarantee the conservation of the transverse emittance of the witness [13]. Further, the accelerating field is uniform across the hollow channel, allowing monoenergetic acceleration. A high quality witness bunch is vital for a number of applications, such as future high-energy colliders [14] or XFEL machines [15]. Thus, hollow-plasma-channel acceleration appears the perfect candidate for next-generation particle accelerators.

Unfortunately, hollow plasma channels suffer from a severe drawback - the beam-breakup (BBU) instability [16, 17]. As a charged bunch propagates in a hollow channel, plasma electrons in the channel wall respond. The resulting space-charge results in an attractive force between the bunch and the wall. The plasma response increases as the bunch moves towards the wall, increasing the attractive force. This instability manifests as a hosing of the beam: an oscillation of the beam centroid along its length [18]. Ultimately, the bunch tail hits the wall of the channel and the bunch is destroyed. The characteristic growth distance of the BBU instability is sufficiently

short that no significant energy exchange from the driver to the wake can be achieved before the driver is lost. A similar instability is observed in dielectric-based accelerators [19].

BBU is well known in other acceleration schemes. In conventional linear accelerators [20] it is controlled through BNS-stabilization [21], in which an energy chirp is applied to the bunch. The resulting head-to-tail chirp in the betatron frequency breaks the resonance between the beam and channel, suppressing the instability. The chirp must be consistent with the focusing properties of the quadrupole guiding structure [22], and must be maintained over the whole accelerating/decelerating distance. Recently, BNS stabilization has been successfully applied to dielectric-based accelerating structures [23]. However, even with current state-of-the-art magnetic quadrupole technology, offering field gradients on the order of 1 T/mm, the attainable accelerating field is limited to a few 100 MV/m. The presence of the instability places fundamental constraints on the maximum accelerating field [24].

In the blowout regime of plasma wakefield acceleration, the BBU growth rate is significantly smaller than for a hollow channel due to the bubble geometry [25]. This allows stabilization to be achieved by using a drive beam with an initial energy spread [26] or large transverse size [27], or even through driver energy loss [26]. These methods are either inapplicable or insufficient for the stabilization of the hollow channel. However, the driver length in the blowout regime is necessarily limited by the bubble length, which places an upper limit on the transformer ratio, and so the efficiency. In a hollow channel, the driver length is limited only by the BBU instability.

Here we show that stable acceleration in a hollow plasma channel can be achieved through the inclusion of a thin co-axial plasma filament. The accelerator configuration is shown in Fig. 1. We assume the plasma density n in the filament to be the same as in the walls of the channel. The filament radius r_f must be small, so that $k_p r_f \ll 1$. Here $k_p = \omega_p/c$ is the characteristic plasma wave number, with $\omega_p = \sqrt{4\pi n e^2/m}$ is the corresponding electron plasma frequency. If we use an electron drive bunch with a current $I_d \gg I_A (k_p r_f)^2$, where $I_A =$

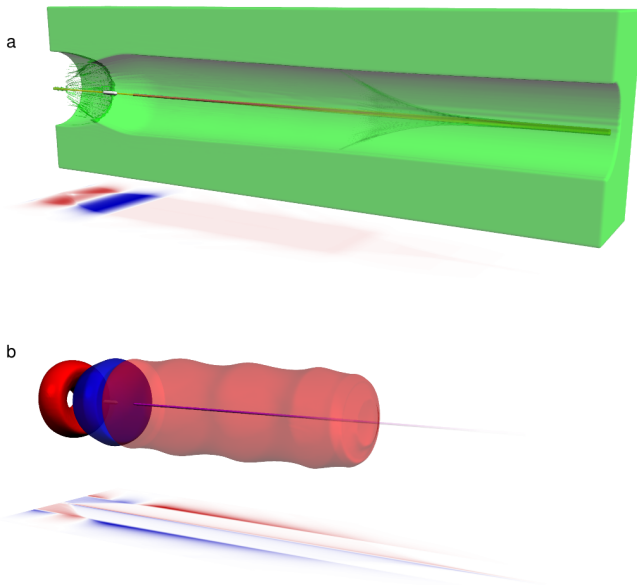


Figure 1. Configuration of the co-axial-channel accelerator. a) A drive beam (purple) propagates in a hollow channel, scattering the plasma electrons (green) from the co-axial filament, leaving an ion column (yellow). The response of the bulk plasma generates a longitudinal electric field, shown as a 2D cut through the axis projected underneath. This field allows the acceleration of a witness bunch (white) to energies much higher than that of the driver. b) Field configuration, showing isosurfaces of the decelerating field acting on the driver (translucent red, at $0.01E_c$, where $E_c = \omega_p m/e = 23$ GV/m); the accelerating field acting on the witness (blue, $-0.1E_c$); and the field suitable for the acceleration of positrons (red, $0.1E_c$). The driver and witness are also shown, for easy comparison to (a). The projection underneath shows a 2D cut through the axis of the transverse field $E_y - B_z$ acting on the driver and witness.

$mc^3/e = 17$ kA is the natural current unit, the transverse self-field of the driver will scatter the plasma electrons from the filament. The remaining ion column will guide both the electron driver and a negatively charged witness. Simultaneously, the ion column will slowly pinch due to the high charge of the drive beam. The characteristic pinch time is $\tau_i \sim (r_f/c) \sqrt{MI_A/ZmI_d}$, where M is the ion mass and Z is the ion charge. As the ion pinch begins at the head of the driver, the ion density, and so the effective betatron frequency, increases along the length of the beam. The large effective chirp guarantees the bunch stability through the BNS mechanism [21, 22], even for a monoenergetic driver. This chirp is independent of the beam energy, allowing much larger chirp rates than can be achieved by tailoring the driver energy spread. This makes the configuration ideal for exploiting the large acceleration gradients possible in a plasma accelerator.

To demonstrate stable acceleration in a co-axial chan-

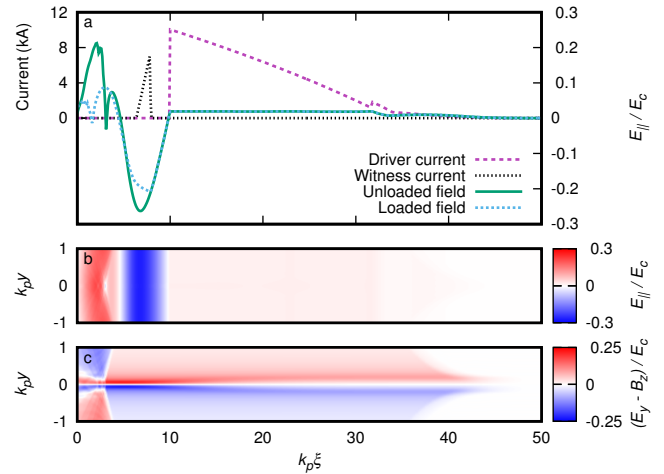


Figure 2. Beam profiles and wakefields. a) Initial drive- and witness-beam currents and the on-axis longitudinal field, plotted in the co-moving coordinate $\xi = z - ct$. The maximum decelerating field inside the drive beam is $E_- = 0.019E_c$. The maximum unloaded accelerating field reaches $E_+^{\text{unloaded}} = -0.26E_c$, corresponding to an unloaded transformer ratio of 13.6. When loaded with the witness bunch, the accelerating field flattens to $\langle E_+^{\text{loaded}} \rangle = -0.2E_c \approx 4.6$ GV/m. b) A 2D cut of the longitudinal field, E_{\parallel} , through the axis. c) A 2D cut of the transverse field $(E_y - B_z)/E_c$ through the axis.

nel, we use the fully three-dimensional quasi-static particle-in-cell code qv3d, developed on the platform of the VLPL code [28]. This makes possible simulations that would be infeasible using conventional simulation methods [29]. We choose helium as the background gas with an atomic density $n = 5.7 \times 10^{16} \text{ cm}^{-3}$. The hollow plasma channel has a radius $k_p r_c = 3$, and the on-axis plasma filament has a radius $k_p r_f = 0.2$. In dimensional units, these are $r_c = 67 \mu\text{m}$ and $r_f = 4.4 \mu\text{m}$. The filament and channel walls are taken to be singly ionized. We do not discuss here how such a plasma configuration may best be achieved. The standard method to create a hollow channel is by laser ionization [17]. The co-axial filament could, for example, be ionized by a higher-order laser mode or even by the self-field of the drive bunch [30].

Both the driver and witness have an initial particle energy of 2 GeV, a negligibly small energy spread, and an emittance of $1 \mu\text{m}$. The driver consists of two bunches. The main driver has a ramped density profile, with a current increasing from zero to 10 kA over $530 \mu\text{m}$, and a Gaussian transverse profile with $\sigma_{\perp} = 1.6 \mu\text{m}$. This bunch duration is approximately equal to the characteristic pinch time for the ion column.

Such ramped density profiles minimize the decelerating field acting on the driver [31], allowing a larger transformer ratio. However, the high-current driver used here modifies the equilibrium radius of the channel and induces a return current in the bulk plasma. This results

in a larger effective accelerator loss factor [16] for higher beam currents, i.e. a stronger coupling between the drive beam and the channel. The optimal gradient for the main drive bunch is therefore sublinear. We here make use of a logarithmic ramp profile $I(x) \sim \log(1 + \alpha x/L)$, with $\alpha = 0.057$, which corresponds to a first-order correction to the plasma response.

An additional nonlinear wake term arises due to the scattering of electrons from the on-axis filament. This increases the decelerating field near the leading edge of the driver, reducing the transformer ratio obtained from commonly-used driver profiles, e.g. the double-triangular bunch [32]. We avoid this limitation through the use of a second drive bunch which precedes the main driver, scattering the filament electrons before the peak decelerating field is reached. The leading bunch has a Gaussian rise, $\sigma_{\parallel} = 110 \mu\text{m}$, with a sharp cut to zero at its peak of 610 A. The transverse profile is the same as the main driver. The two drive bunches partially overlap, with the start of the main driver $50 \mu\text{m}$ before the peak of the preceding bunch.

The combined current profile of the two drive bunches, and the resulting wakefield, is shown in Fig. 2a. The maximum decelerating field is $E_- = 0.019E_c$, where the critical field $E_c = c\omega_p m/e = 23 \text{ GV/m}$ for the chosen plasma density. The field structure has an unloaded transformer ratio $T_R = 13.6$. This value is 86% of the theoretical maximum for a main drive bunch of this length [33] in a hollow channel of this radius [16]. We note that the decelerating field after the peak is flat to within $\pm 2.3\%$. Further optimization would require a higher-order treatment for the plasma response.

The leading edge of the witness is located $46 \mu\text{m}$ behind the rear edge of driver. Its transverse profile is Gaussian with $\sigma_{\perp} = 0.79 \mu\text{m}$, and a peak current of 7 kA at its leading edge, decreasing linearly over its $33 \mu\text{m}$ length. This density profile is chosen to correctly load the wakefield. The average accelerating field experienced by the witness $\langle E_+ \rangle = -0.2E_c$ corresponds to a loaded transformer ratio $T_R = 10.2$.

The longitudinal (E_{\parallel}) and transverse ($E_y - B_z$) fields near the channel axis are shown for the unloaded accelerator in Figs. 2b and c. The accelerating and focusing fields are The chirp in the transverse focusing field arising from the pinch of the ion column is immediately apparent.

Without the co-axial plasma filament the driver rapidly becomes transversely unstable. The BBU growth observed in the qv3d code is in good agreement with analytical models, as seen in Fig. 3, which compares simulations with the numerical solution of Eq. (13) from reference [16]. The results diverge as the plasma response becomes nonlinear due to the limitations of the analytic model. Without a plasma filament, simulations for the same parameters as used in Fig. 1 show the loss of the witness beam due to BBU over distances as short as

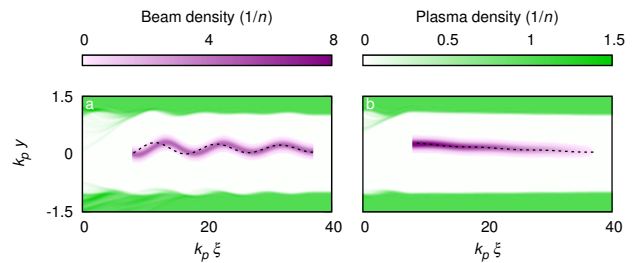


Figure 3. BBU instability. Comparison of the qv3d code (color-map) with a semi-analytical model (black dashed line) for BBU growth in the absence of a co-axial filament. A flat-top (a) and ramped (b) drive beam of average current 200 A propagate $Lk_p = 600$ in a channel of radius $r_c k_p = 1$. The instability is seeded by offsetting the driver by $0.05/k_p$ from the channel axis.

$L_{\text{BBU}} \approx 4000k_p^{-1} \approx 90 \text{ cm}$, limiting the energy gain to $\sim 400 \text{ MeV}$.

The presence of the co-axial plasma filament, however, stabilizes the system so that BBU is avoided completely. We follow the acceleration over a total distance of $L_{\text{acc}} = 2 \times 10^5 k_p^{-1} \approx 4.4 \text{ m}$. The phase-space evolution of the driver is shown in Fig. 4a. We observe that at the end of the acceleration length, the driving bunches have lost $\sim 88\%$ of their total energy.

The phase-space evolution of the witness bunch is shown in Fig. 4b. The witness initially develops a negative energy chirp, in agreement with the field at $L = 0$ shown in Fig. 2. However, as the witness is accelerated, it dephases with the drive beam, and so experiences a non-constant accelerating field over the acceleration length. As we carefully tuned the initial parameters, the gradient of the accelerating field acting on the witness is reversed after an acceleration length of $\sim 1 \text{ m}$, reducing the chirp.

Figure 4c shows the energy spectra of the witness bunch. The energy spread initially increases due to the chirp, and subsequently decreases, reaching a near-monoenergetic peak at $W \approx 21 \text{ GeV}$ for an acceleration distance of $L = 4.4 \text{ m}$. For the witness charge of 410 pC, this corresponds to a total energy of 8.8 J – an energy gain of 8.0 J. Given the initial driver energy of 20 J for the 10 nC beam, this represents a 40% efficiency. Comparing only the energy lost by the driver gives a transfer efficiency of 46%. The measured energy spread $\Delta W = 0.2\%$ is limited by the simulation resolution.

The normalized emittance of the witness grows rapidly at the start of the simulation from $\epsilon^* = 1 \mu\text{m}$ to $1.5 \mu\text{m}$, and shows only slight growth over the acceleration length, reaching $1.8 \mu\text{m}$ after 4.4 m, as seen in Fig 4d. The rapid growth of the initial emittance is likely numerical in nature. The resolution-limited emittance at the start of the simulation is estimated at $1.7 \mu\text{m}$ [34].

The leading edge of the driver expands freely due to its initial emittance, but this leads only to a small perturbation of the wakefield. For longer propagation dis-

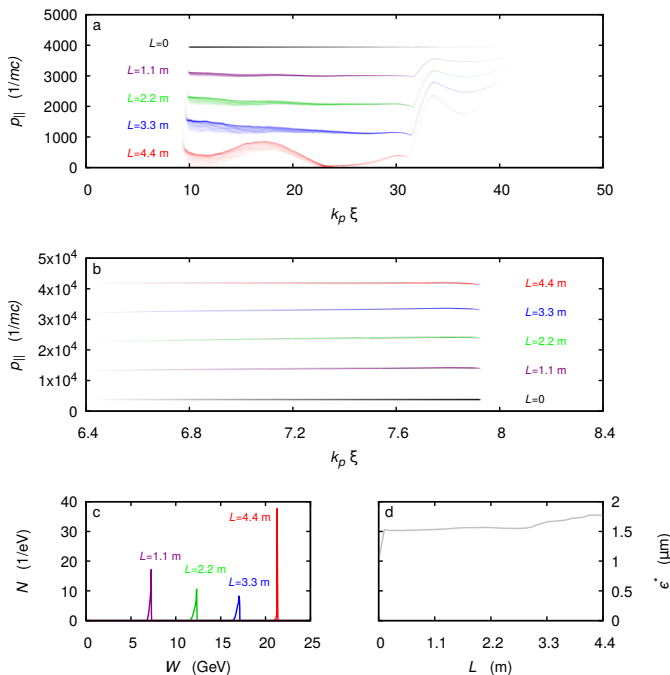


Figure 4. Evolution of the drive and witness beams. a) Longitudinal phase-space density ($p_{||}, \xi$) of the driver after an acceleration length of $L = 0$ (initial distribution), 1.1, 2.2, 3.3, and 4.4 m. At the end of the acceleration, the driver has lost a large fraction of its energy. b) Longitudinal phase space ($p_{||}, \xi$) of the witness at the same positions. Initially, the witness develops a longitudinal chirp. As the witness dephases with the driver, however, the field acting on the witness changes, leading to a reduction in the acquired chirp after ~ 2.8 m. c) Energy spectra of the witness bunch after an acceleration length of $L = 1.1, 2.2, 3.3$ and 4.4 m. The choice of initial witness parameters results in a near-monoenergetic bunch at the end of the acceleration length. d) Evolution of the witness bunch emittance over the entire simulation length. The large initial growth in emittance is likely numerical in nature.

tances, this could be compensated with an external focusing field. Simulations show that the slow pinch of the ion column is vital for beam stabilization - the same configuration with a heavier ion species again results in BBU. Helium also has the desirable property that no secondary ionization occurs for these parameters. Dark current injection is avoided, as electrons streaming back from the bulk plasma behind the driver arrive only after the first potential bucket.

The use of plasma as the acceleration medium makes this acceleration scheme extremely flexible. All lengths scale directly with the plasma wavelength, and so, if desired, a wider channel in a lower-density plasma can be used to give the same acceleration over a longer propagation distance, which may be easier to achieve experimentally. The plasma density used here represents the upper limit for this configuration. At higher densities, the self-field of the driver becomes sufficient to ionize

the bulk gas in the channel. However, it is also possible to make use of a lower-current driver over a longer propagation distance, which reduces the required beam charge. In this case, the optimal shape of the driver will be slightly altered due to the nonlinearity of the plasma response.

Due to the use of an ion-column to focus the beam, this mechanism is only appropriate for an electron driver. However, we note that this configuration could be used to accelerate a positron witness bunch with a donut profile. Electrons from the bulk plasma stream back to compensate the ion filament behind the driver, leading to an inversion of the transverse field a short distance $\ll 1/k_p$ from the axis, as can be seen from Fig. 1c. This results in a stable point at which positrons may be accelerated. Comparing with Fig. 1b shows this point coincides with a large positive wakefield. However, the optimization is somewhat more complex than for an electron witness, and so will be discussed in detail in a separate work.

To conclude, we have shown that the use of a coaxial plasma filament within a hollow plasma channel prevents the development of the beam-breakup instability. In the short term, this configuration may serve as a pre-acceleration scheme for a conventional accelerator, increasing the dipole field strength at injection. Ultimately, though, the ability to stably and efficiently accelerate a witness bunch in a single stage finally offers a path towards a new generation of novel high-energy plasma-based accelerators. The combination of high transformer ratio and monoenergetic acceleration potentially makes this technology a serious contender for applications-driven research.

This work has been supported by the Deutsche Forschungsgemeinschaft and by BMBF.

-
- [1] E. Esarey, C. B. Schroeder, and W. P. Leemans, *Rev. Mod. Phys.* **81**, 1229 (2009).
 - [2] C. Joshi and A. Caldwell, in *Accelerators and Colliders*, edited by S. Myers and H. Schopper (Springer Berlin Heidelberg, Berlin, Heidelberg, 2013) Chap. 12.1, pp. 592–605.
 - [3] A. Pukhov and J. Meyer-ter Vehn, *Appl. Phys. B* **74**, 355 (2002).
 - [4] I. Blumenfeld, C. E. Clayton, F.-J. Decker, M. J. Hogan, C. Huang, R. Ischebeck, R. Iverson, C. Joshi, T. Katsouleas, N. Kirby, W. Lu, K. A. Marsh, W. B. Mori, P. Muggli, E. Oz, R. H. Siemann, D. Walz, and M. Zhou, *Nature* **445**, 741 (2007).
 - [5] S. Steinke, J. van Tilborg, C. Benedetti, C. G. R. Geddes, C. B. Schroeder, J. Daniels, K. K. Swanson, A. J. Gonsalves, K. Nakamura, N. H. Matlis, B. H. Shaw, E. Esarey, and W. P. Leemans, *Nature* **530**, 190 EP (2016).
 - [6] J. B. Rosenzweig, G. Andonian, M. Ferrario, P. Muggli, O. Williams, V. Yakimenko, and K. Xuan, *AIP Conference Proceedings* **1299**, 500 (2010).

- [7] W. Lu, C. Huang, M. Zhou, W. B. Mori, and T. Katsouleas, *Phys. Rev. Lett.* **96**, 165002 (2006).
- [8] A. A. Golovanov, I. Y. Kostyukov, J. Thomas, and A. Pukhov, *Phys. Plasmas* **23**, 093114 (2016).
- [9] A. Pukhov, N. Kumar, T. Tückmantel, A. Upadhyay, K. Lotov, P. Muggli, V. Khudik, C. Siemon, and G. Shvets, *Phys. Rev. Lett.* **107**, 145003 (2011).
- [10] The AWAKE collaboration, *Plasma Phys. Controlled Fusion* **60**, 014046 (2018).
- [11] N. E. Andreev, L. M. Gorbunov, V. I. Kirsanov, K. Nakajima, and A. Ogata, *Phys. Plasmas* **4**, 1145 (1997).
- [12] W. D. Kimura, H. M. Milchberg, P. Muggli, X. Li, and W. B. Mori, *Phys. Rev. ST Accel. Beams* **14**, 041301 (2011).
- [13] L. Yi, B. Shen, L. Ji, K. Lotov, A. Sosedkin, XiaomeiZhang, W. Wang, J. Xu, Y. Shi, L. Zhang, and Z. Xu, *Sci. Rep.* **4**, 4171 (2014).
- [14] T. Behnke, J. E. Brau, B. Foster, J. Fuster, M. Harrison, J. McEwan Paterson, M. Peskin, M. Stanitzki, N. Walker, and H. Yamamoto, *The International Linear Collider Technical Design Report - Volume 1: Executive Summary*, Tech. Rep. (The International Linear Collider, 2013).
- [15] T. Tschentscher, M. Altarelli, R. Brinkmann, T. Delissen, A. Schwarz, and K. Witte, *Synchrotron Radiation News* **19**, 13 (2006).
- [16] C. B. Schroeder, D. H. Whittum, and J. S. Wurtele, *Phys. Rev. Lett.* **82**, 1177 (1999).
- [17] C. A. Lindstrøm, E. Adli, J. M. Allen, W. An, C. Beekman, C. I. Clarke, C. E. Clayton, S. Corde, A. Doche, J. Frederico, S. J. Gessner, S. Z. Green, M. J. Hogan, C. Joshi, M. Litos, W. Lu, K. A. Marsh, W. B. Mori, B. D. O'Shea, N. Vafaei-Najafabadi, and V. Yakimenko, *Phys. Rev. Lett.* **120**, 124802 (2018).
- [18] D. H. Whittum, W. M. Sharp, S. S. Yu, M. Lampe, and G. Joyce, *Phys. Rev. Lett.* **67**, 991 (1991).
- [19] C. Li, W. Gai, C. Jing, J. G. Power, C. X. Tang, and A. Zholents, *Phys. Rev. ST Accel. Beams* **17**, 091302 (2014).
- [20] W. K. H. Panofsky and M. Bander, *Review of Scientific Instruments* **39**, 206 (1968), <https://doi.org/10.1063/1.1683315>.
- [21] V. E. Balakin, A. V. Novokhatsky, and V. P. Smirnov, in *Proceedings, 12th International Conference on High-Energy Accelerators, HEACC 1983: Fermilab, Batavia, August 11-16, 1983*, Vol. C830811 (1983) pp. 119–120.
- [22] G. V. Stupakov, SLAC-AP-108 (1997).
- [23] A. Zholents, W. Gai, S. Doran, R. Lindberg, J. Power, N. Strelnikov, Y. Sun, E. Trakhtenberg, I. Vasserman, C. Jing, A. Kanareykin, Y. Li, Q. Gao, D. Shchegolkov, and E. Simakov, *Nuclear Instruments and Methods in Physics Research Section A: Accelerators, Spectrometers, Detectors and Associated Equipment* **829**, 190 (2016), (2nd European Advanced Accelerator Concepts Workshop - EAAC 2015).
- [24] S. S. Baturin and A. Zholents, *Phys. Rev. Accel. Beams* **21**, 031301 (2018).
- [25] C. Huang, W. Lu, M. Zhou, C. E. Clayton, C. Joshi, W. B. Mori, P. Muggli, S. Deng, E. Oz, T. Katsouleas, M. J. Hogan, I. Blumenfeld, F. J. Decker, R. Ischebeck, R. H. Iverson, N. A. Kirby, and D. Walz, *Phys. Rev. Lett.* **99**, 255001 (2007).
- [26] T. J. Mehrling, R. A. Fonseca, A. Martinez de la Ossa, and J. Vieira, *Phys. Rev. Lett.* **118**, 174801 (2017).
- [27] A. Martinez de la Ossa, T. J. Mehrling, and J. Osterhoff, *Phys. Rev. Lett.* **121**, 064803 (2018).
- [28] A. Pukhov, *CERN Yellow Reports* **1**, 181 (2016).
- [29] Simulations were carried out in the light frame, $\xi = z/c - t$, with a resolution of $\Delta_x = \Delta_y = 0.07/k_p$, $\Delta_\xi = 0.1/k_p$, and a simulation box size of $15/k_p \times 15/k_p \times 50/k_p$. The plasma response was modelled with a timestep $\Delta_t = 1000/\omega_p$, with the witness and drive beams subcycled with a timestep $\Delta_t = 10/\omega_p$ in order to correctly resolve the betatron frequency. 4 particles per cell were used for the bulk plasma, 64 for the drive beam and plasma filament, and 4096 for the witness bunch.
- [30] R. Tarkeshian, J. L. Vay, R. Lehe, C. B. Schroeder, E. H. Esarey, T. Feurer, and W. P. Leemans, *Phys. Rev. X* **8**, 021039 (2018).
- [31] K. L. F. Bane, P. Chen, and P. B. Wilson, *IEEE Transactions on Nuclear Science* **32**, 3524 (1985), also published in SLAC-PUB 3662 (1985).
- [32] B. Jiang, C. Jing, P. Schoessow, J. Power, and W. Gai, *Phys. Rev. ST Accel. Beams* **15**, 011301 (2012).
- [33] S. S. Baturin and A. Zholents, *Phys. Rev. Accel. Beams* **20**, 061302 (2017).
- [34] Numerical Cherenkov radiation can lead to nonphysical emittance growth in standard Yee-like PIC codes [35]. However, the quasistatic nature of the qv3d code makes it naturally free from this numerical artefact. The minimum emittance that can be accurately modelled is therefore limited only by the simulation resolution. We consider a particle beam focused down to a radius x_0 , with particles oscillating at the betatron frequency uniformly distributed over all phases. The normalized transverse emittance is then $\gamma\sqrt{\langle x^2 \rangle \langle x'^2 \rangle} = \gamma\sqrt{(x_0^2/3)(\omega_\beta^2 x_0^2/c^2)} = (\omega_\beta \gamma / \sqrt{3}c)x_0^2$. Choosing a beam diameter of one cell, $x_0 = 0.5\Delta_y$, and noting from simulations that the ion column density at the position of the witness is $\sim 6n$ gives the resolution limit for the normalized transverse emittance as $\epsilon^* = 2.7 \times 10^{-8} \sqrt{\gamma}$.
- [35] R. Lehe, A. Lifschitz, C. Thaury, V. Malka, and X. Davoine, *Phys. Rev. ST Accel. Beams* **16**, 021301 (2013).